Supporting Information

Achieving dendrite-free lithium metal anode by a corrosion inhibitor of sodium diethyldithiocarbamate

Yujue Wang[a], Yan Meng[b], Yong Guo*[b] and Dan Xiao*[abc]

[a] *Institute for Advanced Study, Chengdu University, Chengdu 610106, China*

[b] *Institute of New Energy and Low-Carbon Technology (INELT), Sichuan University, Chengdu 610207, China*

[c] *School of Chemical Engineering, Sichuan University, Chengdu 610065, China*

*These are co-corresponding authors.

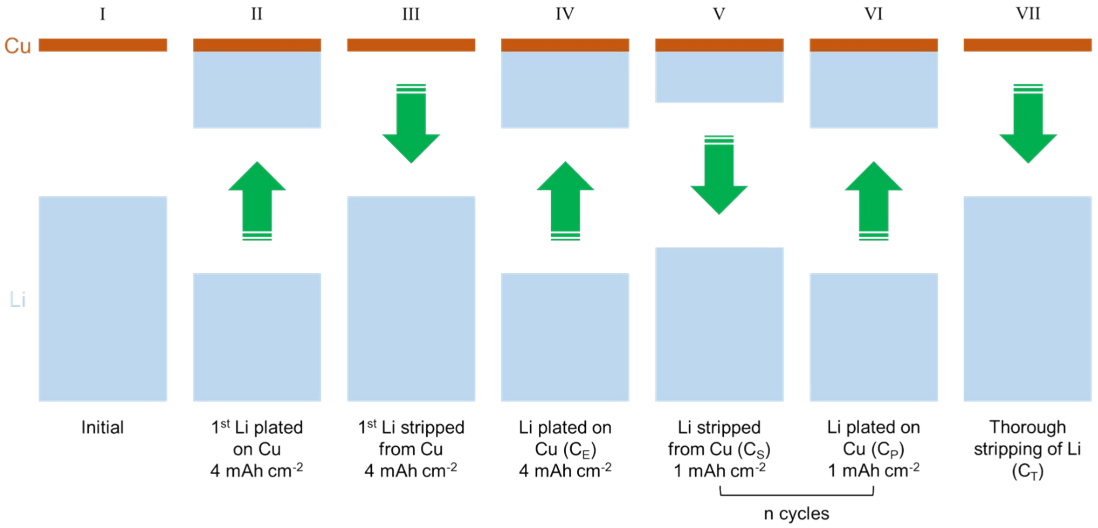

Figure S1. The schematic diagram of plating/stripping cycling Cu||Li asymmetric cell.

In the process of initial Li deposition, irreversible loss of Li is inevitable. Lithium loss involves not only the irreversible reaction between Li and electrolyte to produce by-products, but also the loss caused by the side reaction between Li and Cu matrix. Lithium loss also depends on the composition, surface roughness and surface treatment conditions of the matrix. Although some researchers believe that the solubility of Li in metals such as Cu is very low at room temperature and it will not be alloyed, the oxides on the surface of Cu may occur conversion reaction with Li, resulting in irreversible lithium loss. Therefore, in order to eliminate the influence of Cu surface uncertainty on the Coulombic efficiency of plating/stripping cycles, we carried out a plating/stripping testing method [1] that is conducive to accurate calculation of Coulombic efficiency for asymmetric cells. The testing process is shown in Fig. S1. In the figure, C_E represents the initial excess Li deposition capacity on Cu, which is 8.04 mAh (surface capacity of 4 mAh cm^{-2} and electrode area of 2.01 cm^2), C_P represents the single deposition capacity in the process of n times of repeated Li deposition, which is 2.01 mAh (surface capacity of 1 mAh cm^{-2}), $C_{S,n}$ represents the nth stripping capacity in the process of n repeated Li stripping, C_T represents the capacity of complete Li stripping from Cu. The average Coulombic efficiency (CE_{avg}) in 20 or 100 cycles can be calculated according to the following formula: [1, 2]

$$CE_{avg} = \left(\sum_{i=1}^{n} C_{S,n} + C_T\right) \Big/ \left(nC_P + C_E\right)$$

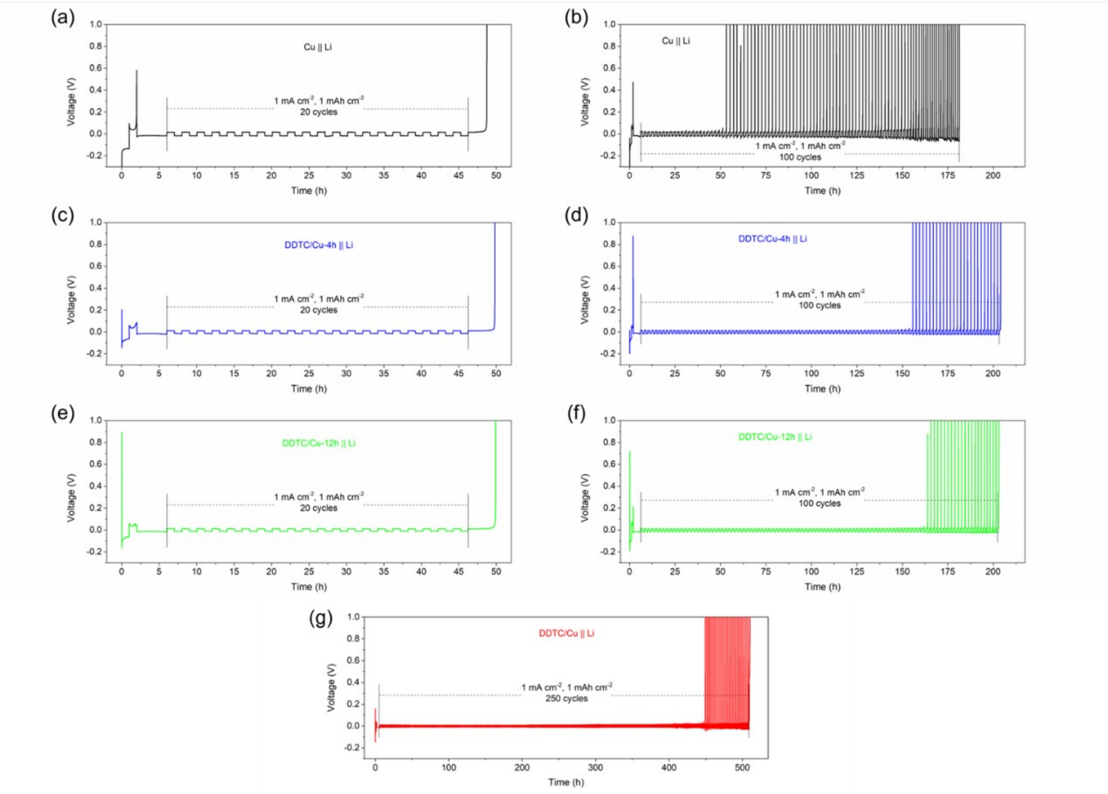

Figure S2. The plating/stripping test results of asymmetric cells using (a, b) bare Cu, (c, d) DDTC/Cu-4h or (e, f) DDTC/Cu-12h electrode with Li foil for 20 or 100 cycles; (g) plating/stripping test results of asymmetric cells using DDTC/Cu-8h electrode for 250 cycles.

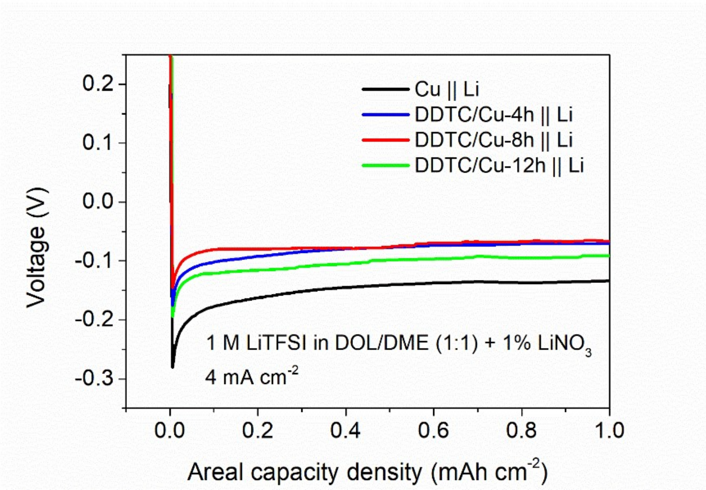

Figure S3. The comparison of initial Li plating voltage profiles of asymmetric cells using bare Cu, DDTC/Cu-4h, DDTC/Cu-8h or DDTC/Cu-12h electrode with Li foil at the current density of 4 mA cm^{-2}.

Table S1. The calculated average Coulombic efficiency of asymmetric cells using bare Cu, DDTC/Cu-4h, DDTC/Cu-8h or DDTC/Cu-12h electrode with Li foil.

Average Coulombic efficiency % Electrode	20 cycles	100 cycles
Bare Cu foil	93.75	72.23
DDTC/Cu-4h	98.22	93.78
DDTC/Cu-8h	99.23	99.15
DDTC/Cu-12h	98.61	92.67

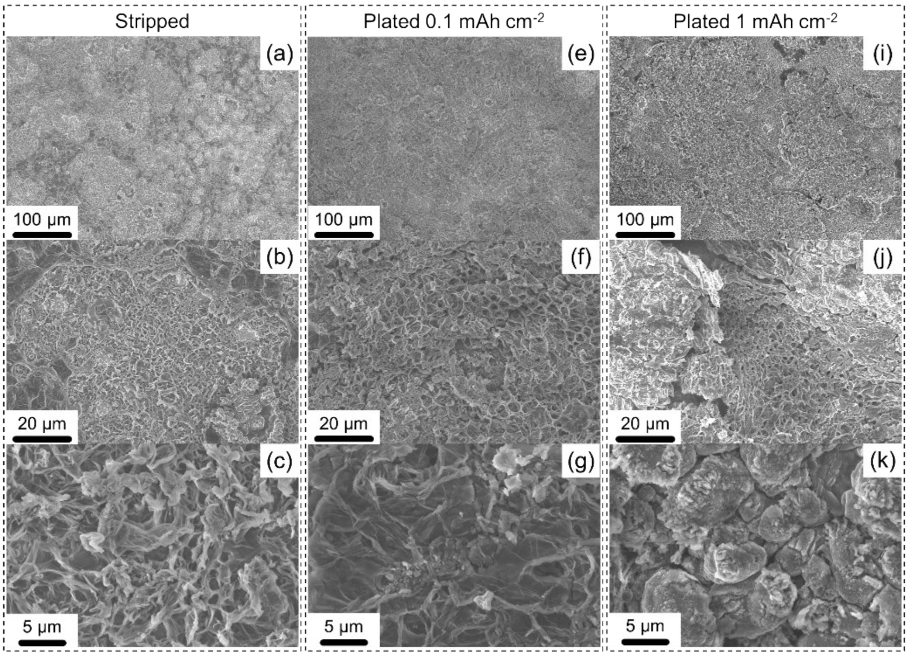

Figure S4. Surface morphology of DDTC/Cu-4h electrode at (a-c) stripped state, (d-f) plating capacity of 0.1 mAh cm^{-2}, and (g-i) plating capacity of 1 mAh cm^{-2} after plating/stripping cycling.

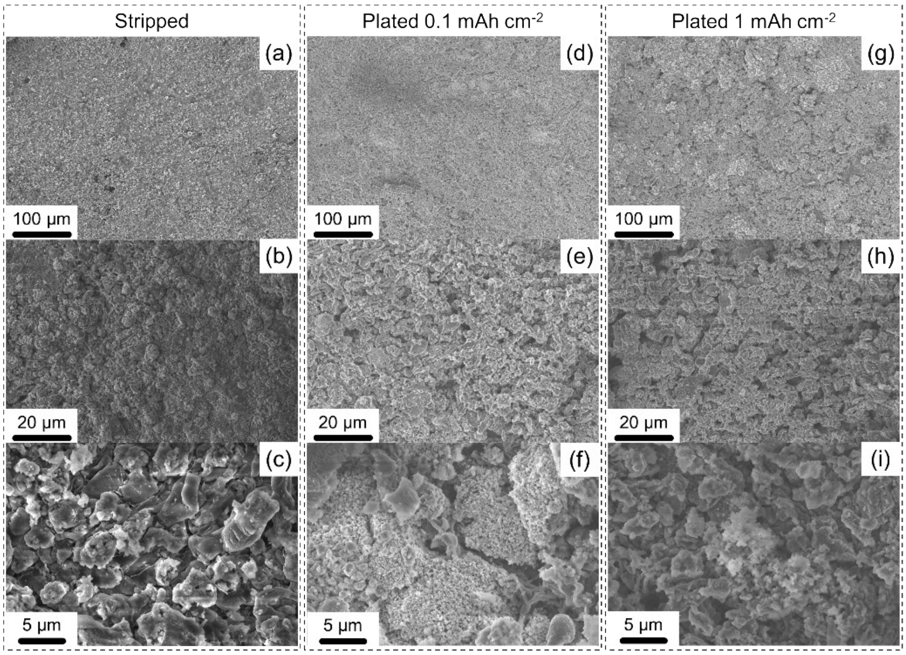

Figure S5. Surface morphology of DDTC/Cu-12h electrode at (a-c) stripped state, (d-f) plating capacity of 0.1 mAh cm^{-2}, and (g-i) plating capacity of 1 mAh cm^{-2} after plating/stripping cycling.

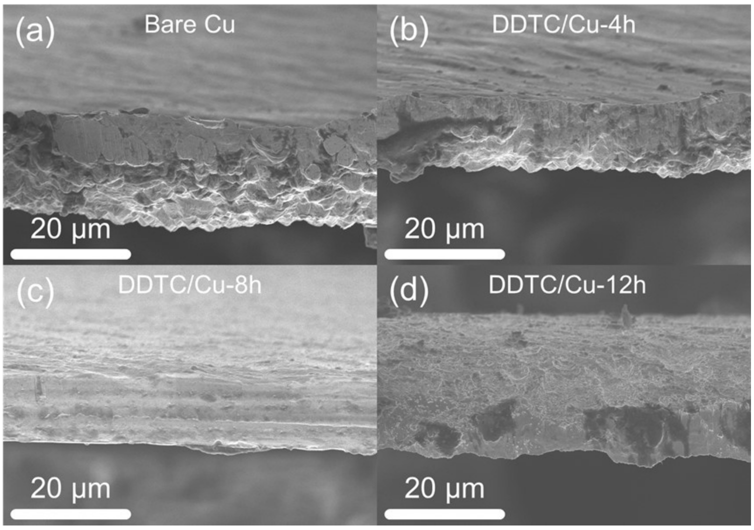

Figure S6. Cross-section SEM of different Cu electrodes.

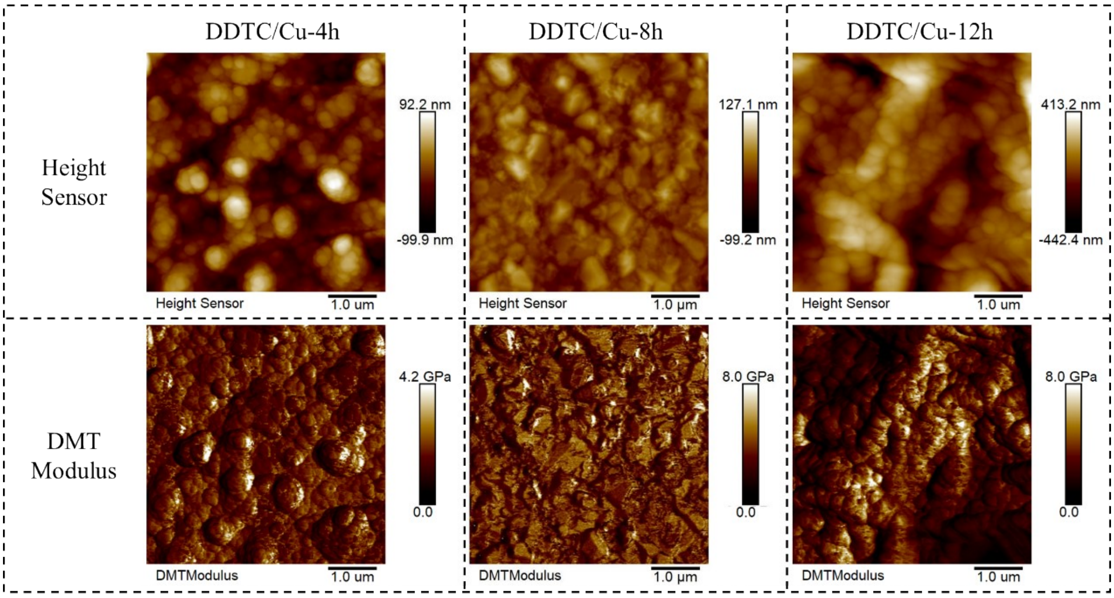

Figure S7. The morphology and Young's modulus distribution of different DDTC surface modified layers.

Table S2. Electronic conductivity of bare Cu, DDTC/Cu-4h, DDTC/Cu-8h and DDTC/Cu-12h

Electronic conductivity (S cm^{-1}) Electrode	Test 1	Test 2	Test 3	Average
Bare Cu foil	5.322	5.327	5.316	5.322
DDTC/Cu-4h	5.313	5.319	5.307	5.313
DDTC/Cu-8h	5.291	5.287	5.286	5.288
DDTC/Cu-12h	4.836	4.817	4.825	4.826

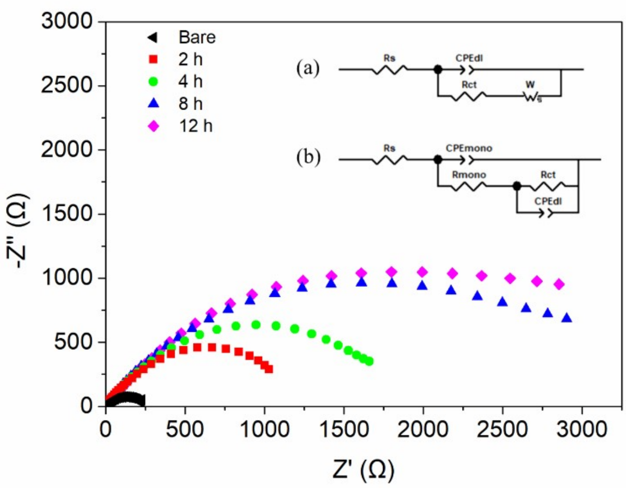

Figure S8. Nyquist plots of different Cu electrodes immersed in 3% NaCl aqueous solution for 4 h after modified by DDTC for different times. Inset is the equivalent circuit models of (a) bare Cu and (b) DDTC modified Cu electrodes.

It is reported that even the modified monolayer without defects cannot completely prevent the transmission of electrons [3]. In fact, self-assembled monolayers always have molecular micropores and defects, through which the corrosion reaction takes place [4]. Fig. S5b is the equivalent circuit used to fit the impedance spectrum of modified electrodes, where, R_s is the solution impedance, R_{mono} is the resistance of self-assembled monolayer, R_{ct} is the charge transfer resistance at electrode interface, W is the Warburg impedance. Considering the influence of metal surface dispersion effect, the constant phase angle element (CPE) replaces the film capacitance and electric double-layer capacitance to fit the impedance data [5-8]. In order to more accurately compare the changes of interface properties between bare Cu and assembled monolayer electrodes, the capacitance value can be obtained by the following formula [9]:

$$C = (Y_0 R^{1-n})^{1/n}$$

Where R is the film resistance or charge transfer resistance; Y_0 is the modulus of film capacitance or electric double layer. The coverage of the self-assembled monolayer can be calculated by the following formula:

$$\eta = \left(1 - \frac{R_{ct}^{0}}{R_{ct}}\right) \times 100$$

Where R_{ct}^{0} and R_{ct} are the charge transfer resistance of bare Cu and modified Cu electrodes, respectively. The values are derived from impedance testing results, which is presented in Table S2. R_{ct} and R_{mono} increase and the CPE_{dl} and CPE_{mono} decrease while extending the DDTC modification time from 2 to 12 h. The coverage η increases from 83.1% to 93.0% in 3% NaCl aqueous solution when the DDTC modification time increases from 2 to 12 h. The coverage at the modification time of 8 and 12 h are similar (92.9% and 93.0, respectively), illustrating that the DDTC modification on Cu surface has reached a saturated state after modification for more than 8 h.

Table S3. EIS parameters of different Cu electrodes immersed in 3% NaCl aqueous solution for 4 h after modified by DDTC for different times.

t (h)	R_s (Ω cm^2)	R_{mono} (Ω cm^2)	CPE_{mono} (μF cm^{-2})	R_{ct} (Ω cm^2)	CPE_{dl} (μF cm^{-2})	W (Ω^{-1} cm^{-2} s$^{0.5}$)	η (%)
Bare	5.189	/	/	154.3	793.2	0.06187	/
2	6.288	109.1	73.76	915.2	193.2	/	83.1
4	10.36	150.6	50.60	1333	136.8	/	88.4
8	9.920	242.6	29.90	2159	92.39	/	92.9
12	14.22	198.2	25.32	2202	94.41	/	93.0

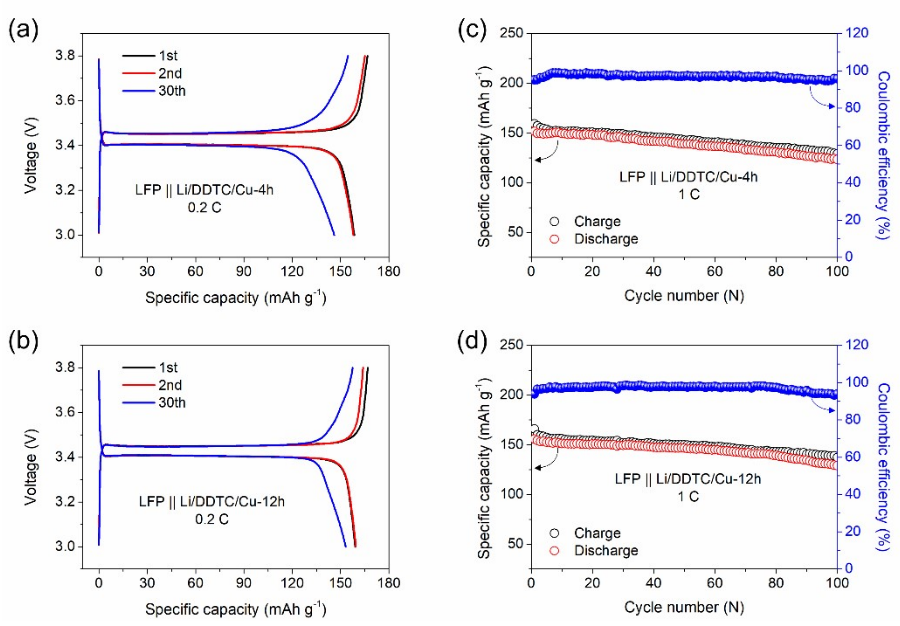

Figure S9. Galvanostatic charge-discharge curves (a, b) and cycling stability with Coulombic efficiency (c, d) of full cells assembled using Li/DDTC/Cu-4h or Li/DDTC/Cu-12h electrode with LFP cathode.

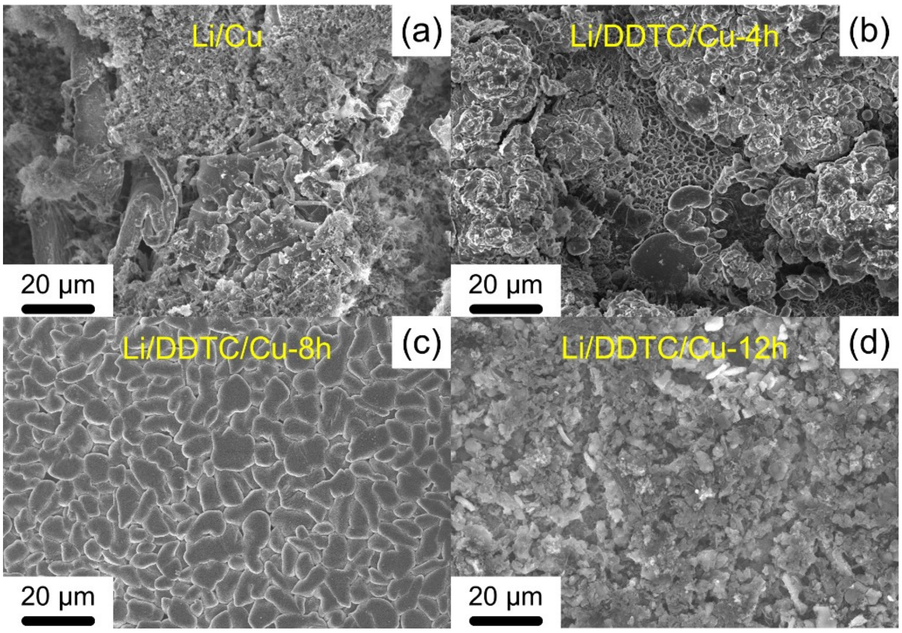

Figure S10. Surface morphology of different Li-loaded electrodes.

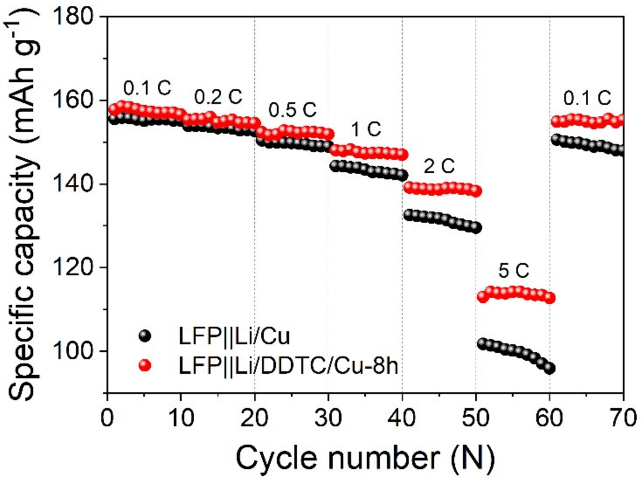

Figure S11. Comparison of rate capability of LFP||Li/DDTC/Cu-8h and LFP||Li/Cu full cells.

Table S4. Comparison of full cell cycling stability to other reported works involving monolayer self-assembly.

Anode	Areal capacity of Li	Areal capacity of cathode	Electrolyte	Cycling stability of full cell
Li/DDTC/Cu (This work)	2 mAh cm^{-2}	0.8 mAh cm^{-2} (LFP)	1 M TFSI in DOL/DME (1:1 vol) with 2% $LiNO_3$	83% retention after 300 cycles
BTA-Cu@Li[10]	3 mAh cm^{-2}	1.5 mAh cm^{-2} (LFP)	1 M TFSI in DOL/DME (1:1 vol) with 2% $LiNO_3$	~30% retention after 220 cycles
OPA-Li-CNT[11]	2.5 mAh cm^{-2}	1.25 mAh cm^{-2} (LFP)	1 M TFSI in DOL/DME (1:1 vol) with 2% $LiNO_3$	82.5% retention after 250 cycles
DHP-Li-CNT[12]	5 mAh cm^{-2}	2.5 mAh cm^{-2} (LFP)	1 M TFSI in DOL/DME (1:1 vol) with 2% $LiNO_3$	~80% retention after 350 cycles
Li@EAM Cu[13]	10 mAh cm^{-2}	2.0 mAh cm^{-2} (LCO)	1 M $LiPF_6$ in PC:FEC:ethyl 2,2,2-trifluoroethyl carbonate (8:1:1, vol) with 10 wt% tris(pentafluorophenyl) borane, 5 wt% $LiBF_4$, and 0.5 wt% $LiNO_3$	87.7% retention after 200 cycles
SAHL-Li[14]	n/a	~1.56 mAh cm^{-2} (S)	1 M TFSI in DOL/DME (1:1 vol)	50% retention after 300 cycles

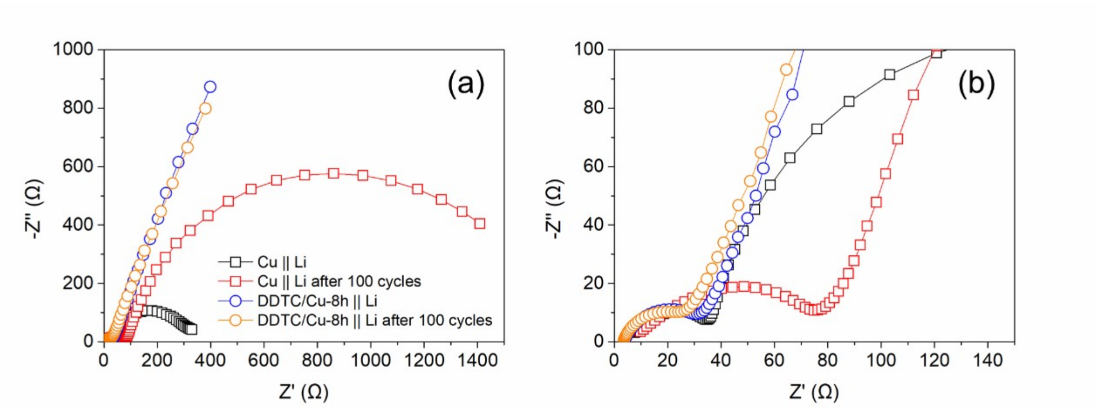

Figure S12. Comparison of the Nyquist plots of Cu||Li and DDTC/Cu-8h||Li before and after cycling. (b) is the local amplification of (a).

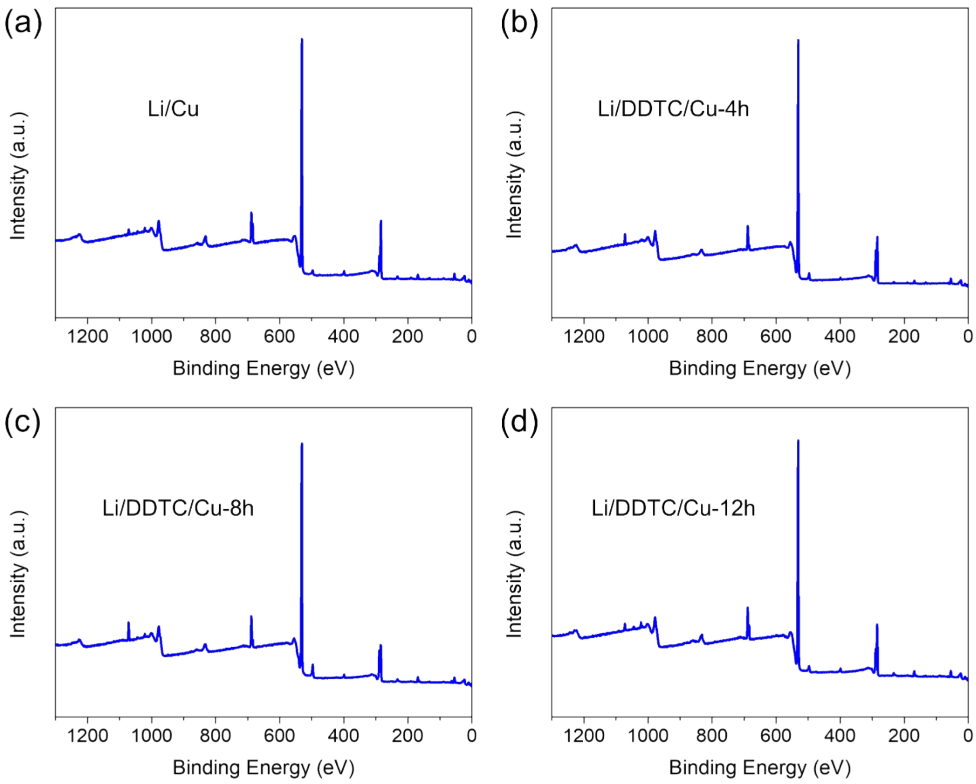

Figure S13. XPS survey spectra of Li/Cu, Li/DDTC/Cu-4h, Li/DDTC/Cu-8h and Li/DDTC/Cu-12h electrodes after cycling.

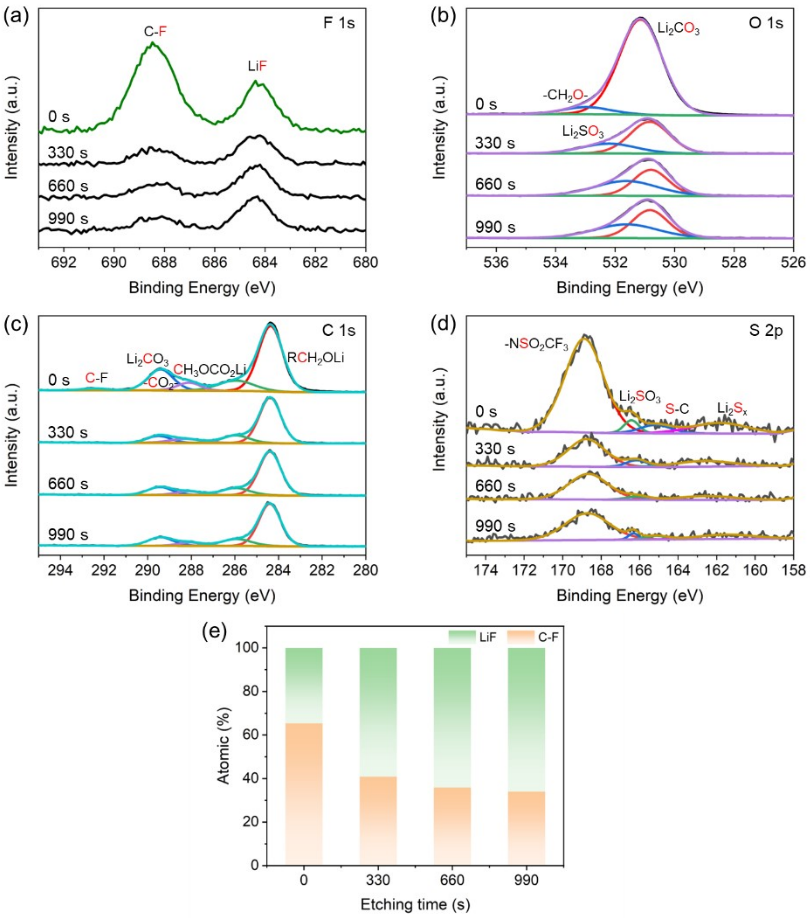

Figure S14. Composition of SEI of Li/Cu electrode after cycling: XPS spectra of F 1s, O 1s, C 1s and S 2p taken after Ar etching for 0 s, 330 s, 660 s and 990 s. (e) The changes of LiF and C-F content in the F 1s spectrum of the SEI of Li/Cu with etching time.

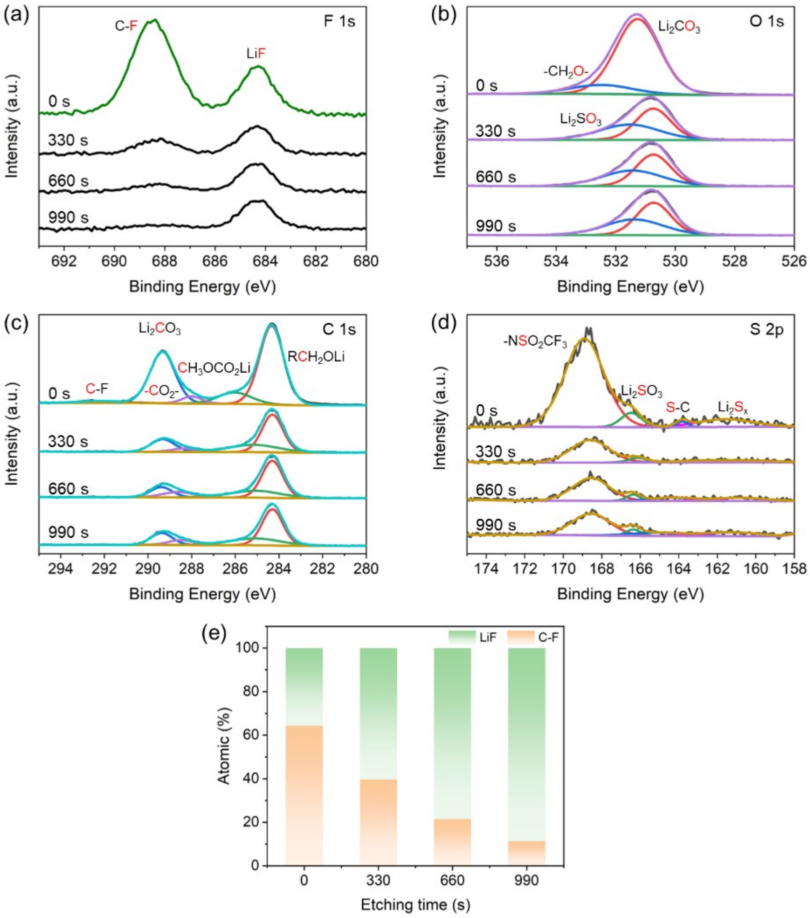

Figure S15. Composition of SEI of Li/DDTC/Cu-4h electrode after cycling: XPS spectra of F 1s, O 1s, C 1s and S 2p taken after Ar etching for 0 s, 330 s, 660 s and 990 s. (e) The changes of LiF and C-F content in the F 1s spectrum of the SEI of Li/DDTC/Cu-4h with etching time.

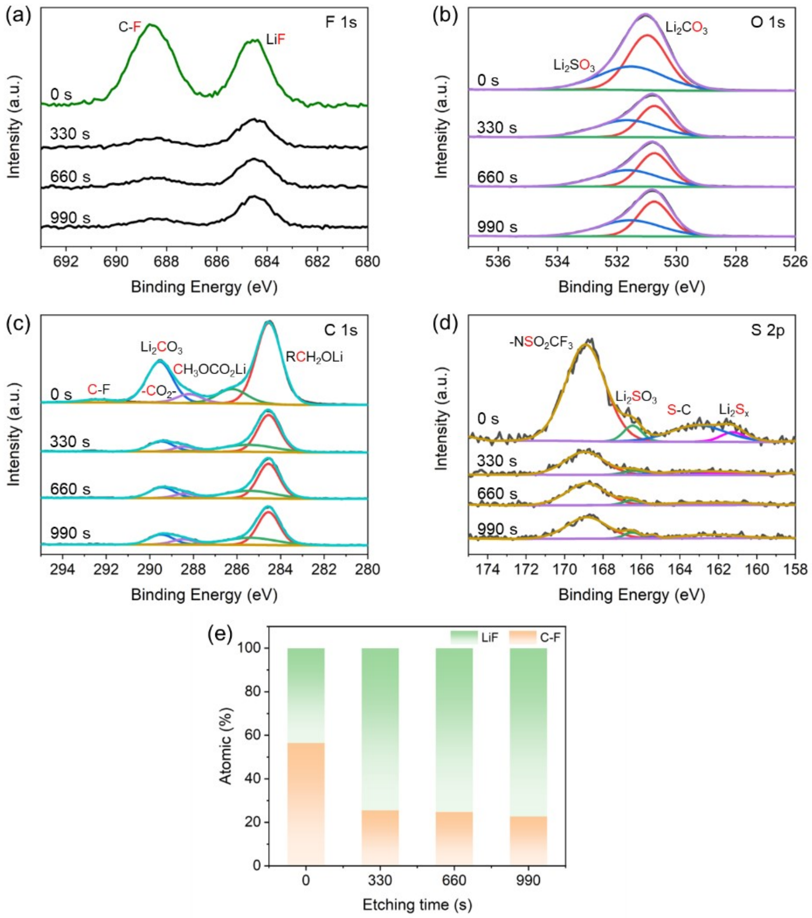

Figure S16. Composition of SEI of Li/DDTC/Cu-12h electrode after cycling: XPS spectra of F 1s, O 1s, C 1s and S 2p taken after Ar etching for 0 s, 330 s, 660 s and 990 s. (e) The changes of LiF and C-F content in the F 1s spectrum of the SEI of Li/DDTC/Cu-12h with etching time.

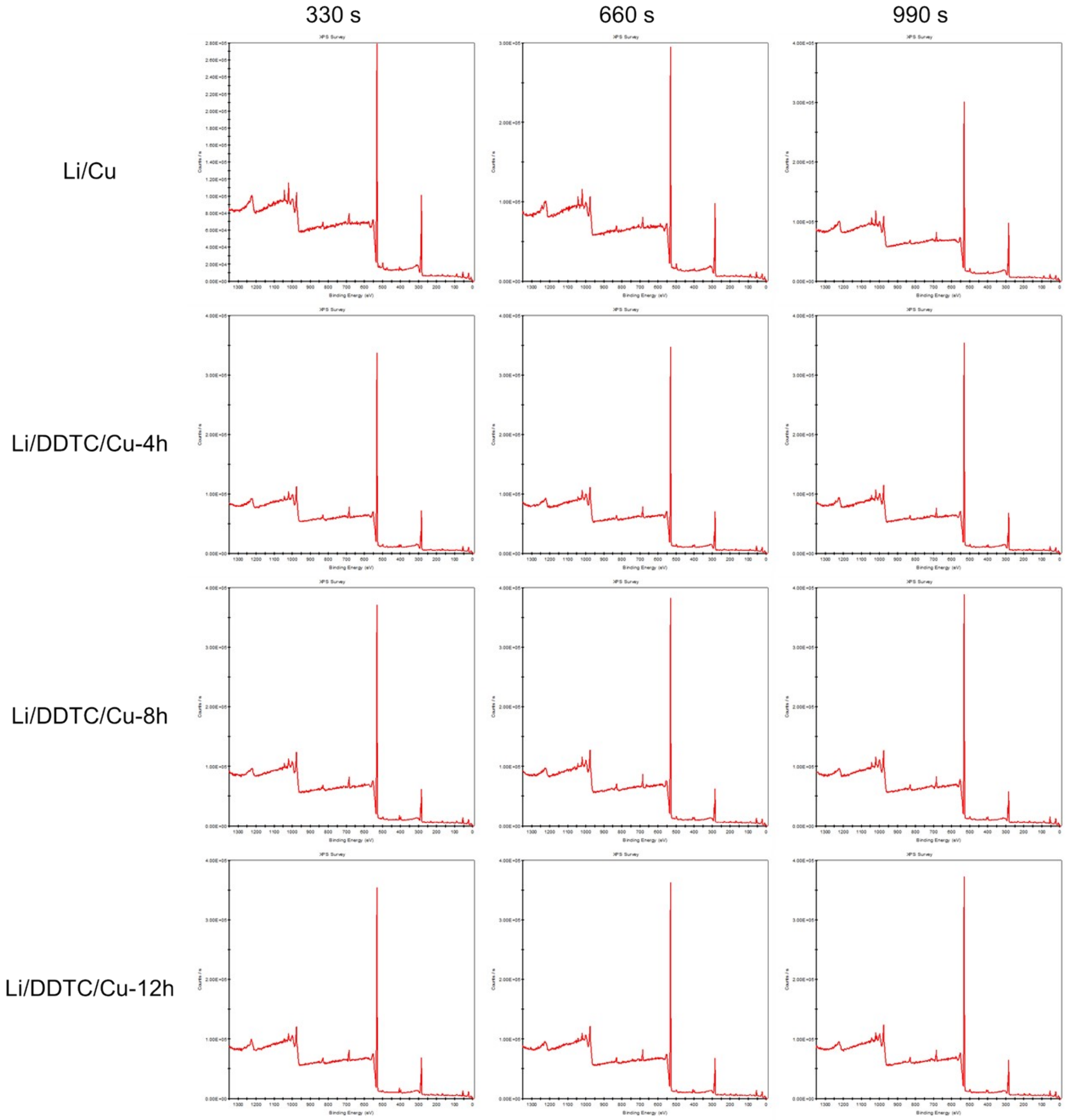

Figure S17. XPS survey spectra of Li/Cu, Li/DDTC/Cu-4h, Li/DDTC/Cu-8h and Li/DDTC/Cu-12h taken after Ar etching for 330 s, 660 s and 990 s, respectively.

References

[1] B.D. Adams, J. Zheng, X. Ren, W. Xu, J.G. Zhang, Accurate determination of Coulombic efficiency for lithium metal anodes and lithium metal batteries, Adv. Energy Mater., 2018, 8, 1702097.

[2] J. Xiao, Q. Li, Y. Bi, M. Cai, B. Dunn, T. Glossmann, J. Liu, T. Osaka, R. Sugiura, B. Wu,

Understanding and applying coulombic efficiency in lithium metal batteries, Nat. Energy, 2020, 5, 561-568.

[3] T.M. Nahir, E.F. Bowden, Impedance spectroscopy of electroinactive thiolate films adsorbed on gold, Electrochim. Acta, 1994, 39, 2347-2352.

[4] J.H. Henríquez-Román, L. Padilla-Campos, M.A. Páez, J.H. Zagal, M.A. Rubio, C.M. Rangel, J. Costamagna, G. Cárdenas-Jirón, The influence of aniline and its derivatives on the corrosion behaviour of copper in acid solution: a theoretical approach, J. Mol. Struct. Theochem, 2005, 757, 1-7.

[5] B.A. Rao, M.Y. Iqbal, B. Sreedhar, Self-assembled monolayer of 2-(octadecylthio) benzothiazole for corrosion protection of copper, Corros. Sci., 2009, 51, 1441-1452.

[6] E. Abelev, D. Starosvetsky, Y. Ein-Eli, Enhanced copper surface protection in aqueous solutions containing short-chain alkanoic acid potassium salts, Langmuir, 2007, 23, 11281-11288.

[7] H. Ma, S. Chen, B. Yin, S. Zhao, X. Liu, Impedance spectroscopic study of corrosion inhibition of copper by surfactants in the acidic solutions, Corros. Sci., 2003, 45, 867-882.

[8] A. Popova, S. Raicheva, E. Sokolova, M. Christov, Frequency dispersion of the interfacial impedance at mild steel corrosion in acid media in the presence of benzimidazole derivatives, Langmuir, 1996, 12, 2083-2089.

[9] H. Ma, X. Cheng, G. Li, S. Chen, Z. Quan, S. Zhao, L. Niu, The influence of hydrogen sulfide on corrosion of iron under different conditions, Corros. Sci., 2000, 42, 1669-1683.

[10] T. Kang, J. Zhao, F. Guo, L. Zheng, Y. Mao, C. Wang, Y. Zhao, J. Zhu, Y. Qiu, Y. Shen, Dendrite-free lithium anodes enabled by a commonly used copper antirusting agent, ACS Appl. Mater. Interfaces, 2020, 12, 8168-8175.

[11] T. Kang, Y. Wang, F. Guo, C. Liu, J. Zhao, J. Yang, H. Lin, Y. Qiu, Y. Shen, W. Lu, Self-assembled monolayer enables slurry-coating of Li anode, ACS Central Sci., 2019, 5, 468-476.

[12] L. Zheng, F. Guo, T. Kang, J. Yang, Y. Liu, W. Gu, Y. Zhao, H. Lin, Y. Shen, W. Lu, Highly stable lithium anode enabled by self-assembled monolayer of dihexadecanoalkyl phosphate, Nano Res., 2020, 13, 1324-1331.

[13] Y. Gao, T. Rojas, K. Wang, S. Liu, D. Wang, T. Chen, H. Wang, A.T. Ngo, D. Wang, Low-temperature and high-rate-charging lithium metal batteries enabled by an electrochemically active monolayer-regulated interface, Nat. Energy, 2020, 5, 534-542.

[14] J. Wang, J. Yang, Q. Xiao, J. Zhang, T. Li, L. Jia, Z. Wang, S. Cheng, L. Li, M. Liu, In situ self-assembly of ordered organic/inorganic dual-layered interphase for achieving long-life dendrite-free Li metal anodes in LiFSI-based electrolyte, Adv. Funct. Mater., 2021, 31, 2007434.